Journal of the Korean Physical Society, Vol. 66, No. 10, May 2015, pp. 1511∼1515

Solvothermal Synthesis of CZTS Nanoparticles in Ethanol: Preparation and Characterization

Xinlong YAN* and Xiaoyan HU
School of Chemical Engineering & Technology, China University of Mining and Technology, Xuzhou 221116, China

Sridhar KOMARNENI
Materials Research Institute, the Pennsylvania State University, University Park, PA 16802, USA

(Received 16 March 2015, in final form 2 April 2015)

In this work, a low-cost, non-toxic and convenient one-pot solvothermal route to synthesize Cu_2ZnSnS_4 (CZTS) nanoparticles is reported. The effects of solvothermal temperature and reaction time on the structure, morphology and optical properties of the as-synthesized product were investigated by using X-ray diffraction (XRD), scanning electron microscopy (SEM), transmission electron microscopy (TEM), energy dispersive X-ray analysis (EDX) measurements and X-ray photoelectron spectroscopy (XPS). The results showed that the crystallinity of the CZTS powders was influenced by the solvothermal temperature and reaction time. The band gap of selected CZTS samples was near the optimum value for photovoltaic solar conversion in a single-band-gap device.

PACS numbers: 61.46.Hk, 68.37.Lp, 42.70.-a, 81.16.Be
Keywords: CZTS nanoparticles, Solvothermal synthesis, Optical properties
DOI: 10.3938/jkps.66.1511

I. INTRODUCTION

Copper-based ternary and quaternary semiconductors, such as $Cu(In,Ga)S_2$ and $Cu(In,Ga)Se_2$, have very beneficial properties for photovoltaic applications. However, because of a shortage in the supplied of In and Ga, the related solar-cell production costs will increase in the near future. Alternatively, copper zinc tin sulfide (CZTS), a particularly desirable material, has attracted a great deal of attention for use in efficient light harvesting because it is composed of abundant, environmentally-benign elements and offers advantageous optical and electronic properties [1–4].

Several methods have been employed to deposit CZTS thin films, including direct current/radio-frequency magnetron sputtering deposition [5], thermal evaporation [6], electron beam evaporation [7], sol-gel deposition [8], electrodeposition [9], nanoparticle-based method [10], *etc.* Among them, solution-based methods for the synthesis of thin films by using CZTS nanoparticle inks have been proposed as one of the most promising routes, and they can help decrease the cost of device fabrication due to the non-vacuum environment and low capital expenditure for equipment [11, 12]. The power conversion efficiency of a nanocrystal-based CZTS solar cell has already reached 11.1% as a result of optimization of the synthesis of CZTS nanocrystal inks and the corresponding film engineering [13]. However, most of the reports focused on the preparation of CZTS nanoparticles by using a hot-injection solution method or a solvothermal method [14, 15], and these syntheses require the use of harsh solvents and chemicals. In a typical solution-based synthesis, copper(II), zinc and tin(IV) precursors are combined in an dodecanethiol solvent and injected into a oleylamine or oleic acid solution [14]. Several of these solvents are expensive, unstable and hazardous, posing health risks, and owe incompatible with the environment. Other poison organic ligands, such as ethylenediamine [16,17] and ethylene glycol [18–22], have been used in similar syntheses. The development of a green chemical route for the preparation of this quaternary sulfide compound still remains a challenge. In this work, a low-cost, non-toxic and convenient one-pot method was developed for the preparation of CZTS nanoparticles. Several preparation conditions were explored to optimize the synthesis of CZTS nanoparticles, and the resulting CZTS powders were characterized for phase identity, morphology and band gap.

II. EXPERIMENTS

Copper(II) chloride dihydrate ($CuCl_2{\cdot}2H_2O$, $\geq$ 99.0%), zinc chloride ($ZnCl_2$, $\geq$ 98.0%), tin(II) chlo-

*E-mail: yanxl@cumt.edu.cn

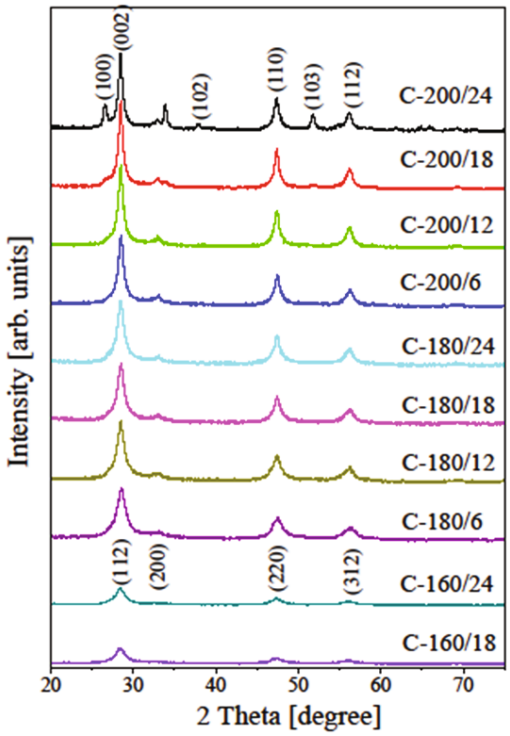

Fig. 1. (Color online) X-ray diffraction patterns of CZTS samples.

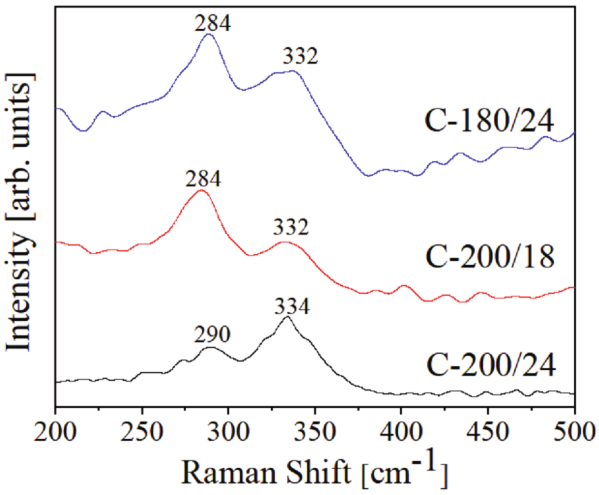

Fig. 2. (Color online) Room-temperature Raman spectra for selected CZTS samples.

ride dihydrate ($SnCl_2{\cdot}2H_2O$, $\geq$ 98%), thiourea (CH_4N_2S, $\geq$ 99.0%) and ethanol ($\geq$ 99.7%) were purchased from Sinopharm Chemical Reagent Co., Ltd., China. All starting materials were used without further purification.

Typically, 2 mmol of $CuCl_2$, 1 mmol of $ZnCl_2$, 1 mmol of $SnCl_2$ and 4 mmol of thiourea were dissolved in 50 mL of ethanol with vigorous stirring. Then, the mixture was purged under nitrogen for 10 min before being transferred into Telflon-lined stainless-steel autoclaves and kept at 200 °C, 180 °C or 160 °C for different times ranging from 6 to 24 h under static conditions. Finally, the precipitates were collected by using centrifugation and washed repeatedly with ethanol. The samples obtained were denoted as C-x/y, where x and y represents the temperature and the time of the solvothermal treatment process, respectively.

Powder X-ray diffraction patterns for the samples were recorded on a Panalytical Xpert PRO X-ray diffractometer with Cu Kα radiation (λ = 1.5406 Å, 40 kV, 40 mA). Raman spectra were recorded using a Bruker Senterra confocal Raman microscope with an excitation wavelength of 532 nm at room temperature. Scanning electron microscopy (SEM) was performed using a FEI Quanta 250 FEG scanning electron microscope (accelerating voltage: 3.0 kV), and elemental mapping was performed using energy-dispersive X-ray spectroscopy (EDX, Bruker Quantax 400). Transmission electron microscopy (TEM) pictures were obtained using a FEI Tecnai G2 F20 device operated at 200 kV. X-ray photoelectron spectroscopy (XPS) was performed using a Thermo Scientific Escalab 250Xi instrument equipped with Al K radiation (hv = 1486.6 eV). Binding energies for the high-resolution spectra were calibrated by setting the C 1s at 284.8 eV. Optical absorption spectra of the samples were measured with a specord 210 plus UV-Vis spectrometer (Analytikjena). The samples were dispersed in ethanol before the measurements.

III. RESULTS AND DISCUSSION

The X-ray diffraction patterns of the CZTS samples prepared at different solvothermal temperatures and times are depicted in Fig. 1. All samples except C-200/24 exhibit peaks at approximately 28.4° (112), 32.9° (200), 47.3° (220), 56.1° (312), which are in good agreement with the high-intensity reflections of bulk kesterite CZTS [23,24], according to the Powder Diffraction File (PDF) 26-0575. With increasing solvothermal temperature and time, the intensity of the peaks increases, indicating that the crystallinity of kesterite CZTS improves as a function of temperature and time whereas the full width at half maximum (FWHM) of the (112) peak decreases, indicating an increase in the particle size. Unexpectedly, the XRD pattern of the C-200/24 sample did not accurately match the standard pattern of kesterite CZTS (JCPDS 26-0575). Instead, the pattern could be indexed to a wurtzite phase of CZTS.

Because some binary and ternary sulfide phases have XRD patterns that coincide with quaternary compounds [25, 26], three selected samples were further characterized by using Raman scattering to confirm the phases. As shown in Fig. 2, the Raman spectra of CZTS sample C-180/24 and C-200/18 can be seen to be quite similar, with two intense Raman shifts at 284 cm^{-1} and

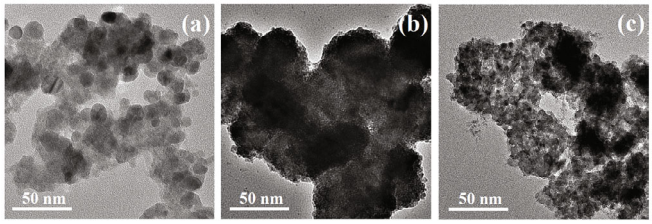

Fig. 3. TEM images of samples (a) C-200/24, (b) C-200/18 and (c) C-180/24.

332 cm^{-1}. For the C-200/24 sample, an intense peak at 334 cm^{-1} and a weak peak at 290 cm^{-1} are observed (Fig. 2). The reported Raman intense peak positions for CZTS are in the range from 331 to 338 cm^{-1} while the weak peak positions are in the range from 284 to 289 cm^{-1} [27–32]. Thus, these results indicate that the CZTS phase was successfully synthesized in an ethanol solution. However, the existence of several weak peaks in the Raman spectra reveals the presence of some minor impurities in these samples.

As Wang *et al.* [33] and Cao *et al.* [34] reported, the valence states of the element Cu, Sn, S changed during the oxidation and the reduction reactions. Apparently, Cu+ chelated with the intermediate product $[SnS_4]^{4-}$ to form $[Cu_2SnS_4]_n{}^{2n-}$, which further reacted with Zn^{2+}, resulting in the formation of Cu_2ZnSnS_4, as described in the following equations:

$$Cu^{2+} + Sn^{2+} \leftrightarrow Cu^{+} + Sn^{4+}, \quad (1)$$

$$S + 2H^{+} \leftrightarrow H_2S + 2e, \quad (2)$$

$$Sn^{4+} + 4H_2S \leftrightarrow [SnS_4]^{4-} + 8H^{+}, \quad (3)$$

$$2Cu^{+} + [SnS_4]^{4-} \leftrightarrow [Cu_2SnS_4]^{2-}, \quad (4)$$

$$Zn^{2+} + [Cu_2SnS_4]^{2-} \leftrightarrow Cu_2ZnSnS_4. \quad (5)$$

The TEM images in Fig. 3(a) and (c) reveal that the sizes of the CZTS nanocrystals in the C-200/24 and the C-180/24 products were ∼9 nm and ∼6 nm, respectively. The size of the nanocrystals increased with increasing solvothermal temperature and time.

Scanning electron micrographs of all samples show aggregated nanoparticles (Fig. 4). Elemental mapping indicate a homogeneous distribution of S, Cu, Sn and Zn in the CTZS nanoparticles. The chemical analysis data suggested that the incorporation of Zn was difficult and, therefore, led to the existence of various minor impurities along with CZTS phases when the syntheses were performed in ethanol. Although the XRD patterns show (vide supra) only a single-phase of CZTS, the formation of the non-stoichiometric chemical composition given above suggests the presence of some amorphous phases in the samples [23].

The valence states of Cu(I), Zn(II), Sn(IV) and S in the sample C-200/24 were determined by using a high-resolution XPS analysis (Fig. 5). In the high-resolution spectrum of Cu 2p, the doublet peaking at 932.4 and 952.3 eV, with a peak splitting of 19.9 eV, is indicative of

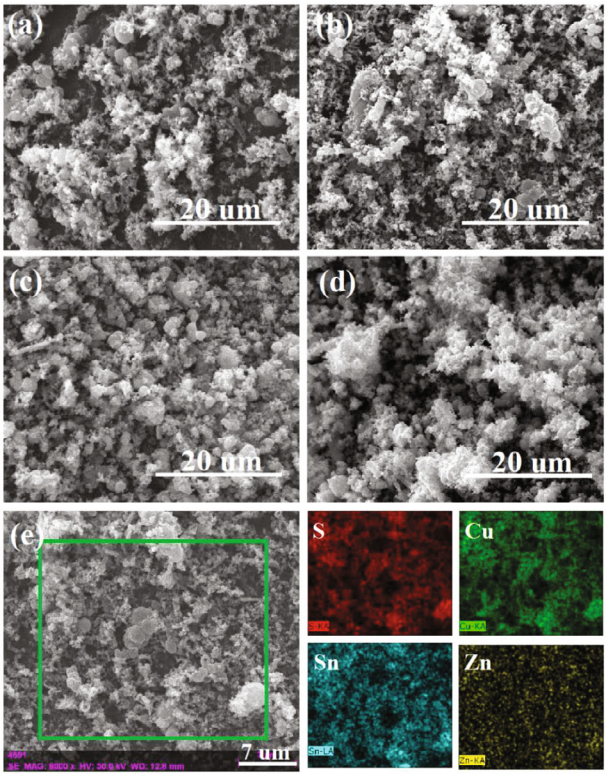

Fig. 4. (Color online) SEM pictures of samples (a) C-200/24, (b) C-200/18, (c) C-180/24, (d) C-160/24 and (e) C-200/24 and corresponding elemental mappings.

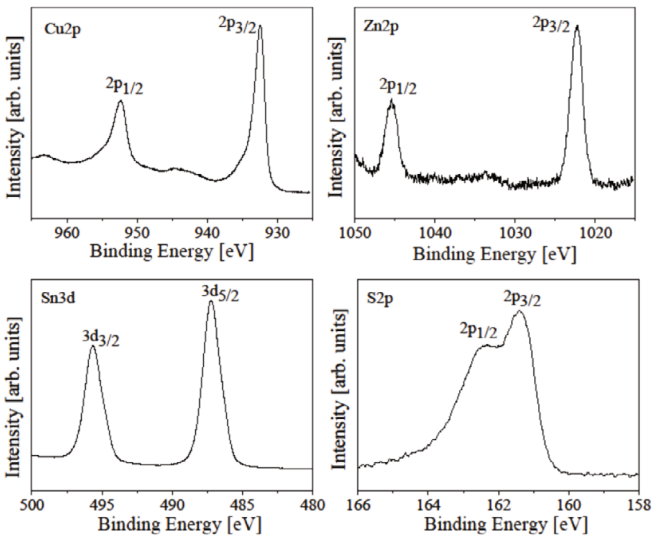

Fig. 5. High-resolution XPS analysis of the four constituent elements in sample C-200/24.

monovalent Cu. The result implies that the Cu^{2+} of the starting material was reduced during the synthesis. The Zn 2p peaks appearing at 1022.3 and 1045.4 eV showed a peak separation of 23.1 eV, which is consistent with the standard splitting of 23.0 eV exhibited by divalent Zn. The peaks located at 487.2 and 495.6 eV, with a peak

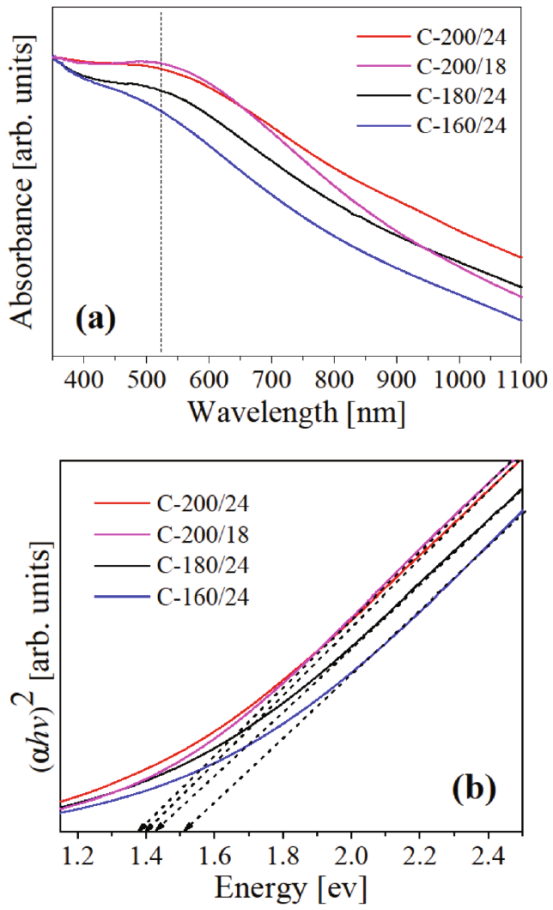

Fig. 6. (Color online) (a) Optical absorption spectra and (b) corresponding band-gap for selected CZTS nanocrystals.

separation of 8.4 eV, can be attributed to tetravalent Sn. The peaks observed at 161.4 and 162.3 eV are in good accordance with those reported for S in sulfide phases. The results suggest a coordination of sulfur with copper, zinc, and tin to form Cu_2ZnSnS_4 [35].

Figure 6(a) shows the absorption spectra of selected CZTS nanocrystals. The synthesized CZTS particles displayed good photo-absorption properties over the entire visible region. This accounts for the black color of the powder sample [36]. A sharp drop in the absorbance was observed for wavenumbers higher than ∼525 nm. At wavenumbers below ∼525 nm, the absorbance increased as the solvothermal temperature was increased from 160 to 200 °C, which may be ascribed to an increase in the crystallite size and a decrease in the number of defects [37]. Because of the formation of impurity phases, the optical adsorption edges shifted slightly to lower energies with increasing solvothermal temperature [38]. The optical band-gap values of the as-synthesized CZTS nanocrystals evaluated from the UV-vis absorption spectra are shown in Fig. 6(b). Plotting $(\alpha hv)^2$ versus hv, where 'α' represents the absorption coefficient and 'hv' is the photon energy, we found the values of the bandgap for the C-200/24, C-200/18, C-180/24 and C-160/24 CZTS samples were 1.38 eV, 1.40 eV, 1.43 eV and 1.52 eV, respectively. These values correspond well with the literature values (∼1.4 − 1.6 eV) [39] and are near the optimum value of 1.45 eV for photovoltaic solar conversion in a single-band-gap device.

IV. CONCLUSION

The CZTS nanoparticles were successfully synthesized by using the solvothermal method using ethanol. With increasing solvothermal temperature and time, the crystallinity of the CZTS samples improved. However, the chemical composition revealed by the EDS analysis suggested the presence of some amorphous phase in these solvothermally prepared samples. The as-prepared samples had a band gap in the range of 1.39 − 1.56 eV, which is close to band gap values of CZTS.

ACKNOWLEDGMENTS

This work was supported by Fundamental Research Funds for Central Universities (No. 2014QNA29), the Natural Science Foundation of Jiangsu Province (No. BK20140182), and the Priority Academic Program Development of Jiangsu Higher Education Institutions.

REFERENCES

[1] A. Walsh, S. Chen, S. H. Wei and X. G. Gong, Adv. Energy Mater. **2**, 400 (2012).
[2] H. Katagiri, K. Saitoh, T. Washio, H. Shinohara, T. Kurumadani and S. Miyajima, Sol. Energy Mat. Sol. C **65**, 141 (2001).
[3] A. I. Inamdar, K. Y. Jeon, H. S. Woo, W. Jung and H. Im, J. Korean Phys. Soc. **60**, 10 (2012).
[4] M. Y. Yeh, Y. F. Huang, C. L. Huang, C. D. Yang, D. S. Wuu and P. H. Lei, J. Korean Phys. Soc. **65**, 196 (2014).
[5] T. Tanaka, T. Nagatomo, D. Kawasaki, M. Nishio, Q. X. Guo, A. Wakahara, A. Yoshida and H. Ogawa, J. Phys. Chem. Solids **66**, 1978 (2005).
[6] A. Redinger and S. Siebentritt, Appl. Phys. Lett. **97**, 092111-1 (2010).
[7] T. Kobayashi, K. Jimbo, K. Tsuchida, S. Shinoda, T. Oyanagi and H. Katagiri, Jpn. J. Appl. Phys. **44**, 783 (2005).
[8] F. Yakuphanoglu, Sol. Energy **85**, 2518 (2011).
[9] H. Araki, Y. Kubo, A. Mikaduki, K. Jimbo, W. S. Maw, H. Katagiri, M. Yamazaki, K. Oishi and A. Takeuchi, Sol. Energy Mater. Sol. Cells **93**, 996 (2009).
[10] S. C. Riha, B. A. Parkinson and A. L. Prieto, J. Am. Chem. Soc. **131**, 12054 (2009).
[11] E. H. Sargent, Nat. Photonics **6**, 133 (2012).
[12] W. C. Liu, B. L. Guo, X. S. Wu, F. M. Zhang, C. L. Mak and K. H. Wong, J. Mater. Chem. A **1**, 3182 (2013).

[13] T. K. Todorov, J. Tang, S. Bag, O. Gunawan, T. Gokmen, Y. Zhu and D. B. Mitzi, Adv. Energy Mater. **3**, 34 (2013).
[14] X. T. Lu, Z. B. Zhuang, Q. Peng and Y. D. Li, Chem. Comm. **47**, 3141 (2011).
[15] Y. Cui, G. Wang and D. C. Pan, J. Mater. Chem. **22**, 12471 (2012).
[16] M. Zhou, Y. Gong, J. Xu, G. Fang, Q. Xu and J. Dong, J. Alloys Comp. **574**, 272 (2013).
[17] M. Cao and Y. Shen, J. Cryst. Growth **318**, 1117 (2011).
[18] L. Shi, C. Pei, Y. Xu and Q. Li, J. Am. Chem. Soc. **133**, 10328 (2011).
[19] Y. L. Zhou, W. H. Zhou, Y. F. Du, M. Li and S. X. Wu, Mater. Lett. **65**, 1535 (2011).
[20] Q. Tian, X. Xu, L. Han, M. Tang, R. Zou, Z. Chen, M. Yu, J. Yang and J. Hu, CrystEngComm. **14**, 3847 (2012).
[21] Y. L. Zhou, W. H. Zhou, M. Li, Y. F. Du and S. X. Wu, J. Phys. Chem. C. **115**, 19632 (2011).
[22] X. Yan, E. Michael, S. Komarneni, J. R. Brownson and Z. Yan, Ceram. Int. **40**, 1985 (2014).
[23] O. Zaberca, A. Gillorin, B. Durand and J. Y. Chane-Ching, J. Mater. Chem. **21**, 6483 (2011).
[24] P. Dai, G. Zhang, Y. Chen, H. Jiang, Z. Feng, Z. Lin and J. Zhan, Chem. Comm. **48**, 3006 (2012).
[25] D. B. Mitzi, O. Gunawan, T. K. Todorov, K. Wang and S. Guha, Sol. Energy Mat. Sol. C **95**, 1421 (2011).
[26] P. A. Fernandes, P. M. P. Salome and A. F. da Cunha, J. Alloys Comp. **509**, 7600 (2011).
[27] M. D. Regulacio, C. Ye, S. H. Lim, M. Bosman, E. Y. Ye, S. Y. Chen, Q. H. Xu and M. Y. Han, Chem. Eur. J. **18**, 3127 (2012).
[28] H. C. Jiang, P. C. Dai, Z. Y. Feng, W. L. Fan and J. H. Zhan, J. Mater. Chem. **22**, 7502 (2012).
[29] L. Shi, C. J. Pei, Y. M. Xu and Q. J. Li, J. Am. Chem. Soc. **133**, 10328 (2011).
[30] S. Ahmed, K. B. Reuter, O. Gunawan, L. Guo, L. T. Romankiw and H. Deligianni, Adv. Energy Mater. **2**, 253 (2012).
[31] M. Li, W. H. Zhou, J. Guo, Y. Zhou, Z. L. Hou, J. Jiao, Z. J. Zhou and S. Wu, J. Phys. Chem. C **116**, 26507 (2012).
[32] S. Sarkar, K. Bhattacharjee, G. C. Das and K. K. Chattopadhyay, CrystEngComm. **16**, 2634 (2014).
[33] Y. Wang, X. J. Liang, Q. Cai, L. Feng, M. G. Shao, J. S. Zhong and W. D. Xiang, Acta Chim. Sinica **70**, 903 (2012).
[34] L. Li, B. L. Zhang, M. Cao, Y. Sun, J. C. Jiang, P. F. Hu, Y. Shen and L. J. Wang. J. Alloys Comp. **551**, 24 (2013).
[35] U. Dasgupta, S. K. Saha and A. J. Pal. Sol. Energy Mat. Sol. C **124**, 79 (2014).
[36] S. Sarkar, K. Bhattacharjee, G. C. Das and K. K. Chattopadhyay, CrystEngComm. **16**, 2634 (2014).
[37] N. M. Shinde, P. R. Deshmukh, S. V. Patil and C. D. Lokhande, Mater. Res. Bull. **48**, 1760 (2013).
[38] M. Suryawanshi *et al.*, Phys. Status Solidi A **211**, 1531 (2014).
[39] X. Zhang, X. Z. Shi, W. C. Ye, C. L. Ma and C. M. Wang, Appl. Phys. A **94**, 381 (2009).